Samir H. Sadek[1]
Francisco Pimenta[2]
Fernando T. Pinho[1]
Manuel A. Alves[2]

[1]CEFT, Departamento de Engenharia Mecânica, Faculdade de Engenharia da Universidade do Porto, Porto, Portugal
[2]CEFT, Departamento de Engenharia Química, Faculdade de Engenharia da Universidade do Porto, Porto, Portugal

Received August 7, 2016
Revised December 7, 2016
Accepted December 8, 2016

Research Article

Measurement of electroosmotic and electrophoretic velocities using pulsed and sinusoidal electric fields

In this work, we explore two methods to simultaneously measure the electroosmotic mobility in microchannels and the electrophoretic mobility of micron-sized tracer particles. The first method is based on imposing a pulsed electric field, which allows to isolate electrophoresis and electroosmosis at the startup and shutdown of the pulse, respectively. In the second method, a sinusoidal electric field is generated and the mobilities are found by minimizing the difference between the measured velocity of tracer particles and the velocity computed from an analytical expression. Both methods produced consistent results using polydimethylsiloxane microchannels and polystyrene micro-particles, provided that the temporal resolution of the particle tracking velocimetry technique used to compute the velocity of the tracer particles is fast enough to resolve the diffusion time-scale based on the characteristic channel length scale. Additionally, we present results with the pulse method for viscoelastic fluids, which show a more complex transient response with significant velocity overshoots and undershoots after the start and the end of the applied electric pulse, respectively.

Keywords:
Electroosmotic mobility / Electrophoretic mobility / Particle tracking velocimetry / Zeta-potential measurement
DOI 10.1002/elps.201600368

Additional supporting information may be found in the online version of this article at the publisher's web-site

1 Introduction

Tracer particles (TP) are often used in microfluidics, including fluid flow visualization and velocimetry techniques. In pressure-driven flows only one main driving force is usually present, while in electrokinetic flows several forces can simultaneously act on the TP and quantifying each contribution can be challenging [1].

Chemical equilibrium between channel walls, or TP surface, and surrounding fluid leads to spontaneous charge separation both at the solid and liquid near their interface. On the liquid side, a thin layer of ions forms near the walls/TP–the electric double layer (EDL)–whereas the fluid elsewhere remains essentially neutral. Applying an external electric field between the inlet and outlet of the channel results in transport by electroosmosis (EO). The motion of the ions in the diffuse layer of the channel walls EDLs, under the action of the electric field, and the subsequent dragging of the bulk of the fluid by shear forces, generates a plug-like flow provided there are no pressure gradient effects as in an open channel without streamwise gradients of electrokinetic properties. The micron-sized particles dispersed in the fluid will be dragged by the moving fluid, but simultaneously the applied electric field results in a force acting on the particle leading to an additional velocity component known as electrophoresis (EP). Hence, the velocity of TP will be the result of both EO and EP contributions.

Both the direction and the intensity of EO and EP velocities depend on an important surface property known as the zeta-potential. The zeta-potential of a given material depends on the properties of the electrolyte which is in contact with the surface, such as its ionic species, the ionic strength, or the medium pH.

Correspondence: Dr. Manuel A. Alves, CEFT, Departamento de Engenharia Química, Faculdade de Engenharia da Universidade do Porto, Rua Dr. Roberto Frias, 4200-465 Porto, Portugal
E-mail: mmalves@fe.up.pt
Fax: +351-22-508-1449

Abbreviations: EDL, Electric double layer; **EO**, Electroosmosis; **EP**, Electrophoresis; **PAA**, Polyacrylamide; **PIV**, Particle image velocimetry; **PTV**, Particle tracking velocimetry; **TP**, Tracer particle

Colour Online: See the article online to view Figs. 5 and 12 in colour.

Several methods are available to measure the zeta-potential, and a brief review will be presented in what follows. From early times the rectangular microchannel, often called the micro-electrophoresis cell [2–5], has been the geometry of choice to determine the zeta-potential from the direct measurement of the EP velocity in Newtonian fluid flows. Initially it has been used in the configuration of a closed cell [5–7] under the forcing imposed by a direct current (DC) electric field, which causes the solution to recirculate: the positively-charged solution close to the wall moves toward the cathode by EO and the solution near the cell center moves towards the anode to maintain conservation of mass, i.e., the closed cell induces a back-pressure gradient. When the flow reaches steady-state, the velocity profile is obtained through tracking the velocity of tracer particles at several depths, and the zeta-potentials of channel walls and tracer particles are obtained by minimization of the error between the measured velocities and the analytical velocity profiles.

The so-called "two-particle correlation method" [8] uses two types of tracer particles with different zeta-potentials and electric properties (different surfaces), but identical size, in order to measure the EO velocity from correlation functions. The correlation functions are initially obtained for the same particles in controlled channel flow experiments under the action of DC electric fields that measure independently the velocity of TPs and the EO velocity. A good agreement between this method and the results from experiments using a fluorescent dye, and numerical simulations, were observed in channels of different materials and shapes. The fluorescent dye method is an alternative technique [8] to directly measure the EO velocity of a solution in a channel under the action of a DC electric field. Only the fluid in the upstream reservoir contains the fluorescent dye and tracking the velocity of the fluid interface at the center of the open channel provides the EO velocity.

Another method to determine experimentally the channel wall zeta-potential is based on imposing a time-periodic electric field in a T-channel [9]: at a suitable frequency range, the oscillation amplitude of the confluent streams, one of which contains a fluorescent dye, is a monotonic function of the zeta-potential. It is an elaborate indirect method to estimate the zeta-potential, based on an experimental measurement with the aid of 3-D numerical simulation to convert the amplitude of oscillation into a zeta-potential.

The current monitoring method [10–12] is a commonly used technique to determine the electroosmotic velocity through the measured slope of the electric current versus time, which together with the Smoluchowski equation [11,12] allows the quantification of the zeta-potential at the channel walls. This method is based on the measurement of the variation with time of the electric current in a capillary flow as one EO flowing electrolyte is completely displaced by a second electrolyte having a slightly different electric conductivity (this slight difference is enough to change the current intensity while keeping the electroosmotic velocity and zeta-potential unchanged). Thus, it is an indirect measuring method, requires at least two electrolytes and the complete replacement of one electrolyte by another can be lengthy, causing Joule-heating effects, which can negatively affect the results.

Micro-particle image velocimetry (micro-PIV) is often used to measure the velocity of suspended tracer particles in microfluidics and it is no surprise that it has also been used to determine electrokinetic flow properties [13–17]. In the high-resolution (in space and time) transient micro-PIV method, Yan et al. [13, 14] used two pulsed lasers to illuminate the tracer particles at the same frequency, but with a fixed small time delay δt between them. Each pair of images, captured by a standard CCD camera, or an sCMOS sensor, over that time delay are then cross-correlated to obtain the displacement and corresponding velocities of the tracer particles. With a standard camera and given the fast time responses of EP and EO velocities, discriminating between these two electrokinetic velocities requires a precise synchronization of voltage switching, laser illumination and camera triggering. This approach measures the particle velocity during the flow startup, when EP is already fully-developed and EO is only starting to propagate by diffusion from the walls towards the channel centerline. The EO velocity is computed from the difference between the steady-state particle velocity and the EP velocity measured at short times, and zeta-potential values are then computed from the corresponding mobilities, following the appropriate Helmholtz-Smoluchowski theory [18,19]. Based on the same principle, but now relying on a high-speed camera, Sureda et al. [16] used also the time-resolved micro-PIV technique to determine the zeta-potential of both the TP and the channel walls.

The micro-PIV technique was again used by Yan et al. [15] to determine the zeta-potentials of TPs and channel wall from velocity profiles measured on both steady flows in open and closed channels, the latter imposing a pressure gradient from mass conservation. In this elaborate method they used a least-squares fitting procedure to determine the best-fit values for the particle velocity and the channel wall zeta-potential, through minimization of the sum of the square of the error between the experimental data and predicted values (from analytical expressions).

Miller et al. [17] derived an analytical expression for the transient startup EO flow with pressure gradient effects, from which five different periods of flow were identified until the flow reached steady-state. Their 2D analytic solution was validated with experimental data obtained by a time-resolved micro-PIV relying on a high-speed camera, for which the effect of electrophoresis on the tracer particles had to be taken into consideration (the high-speed camera allowed the measurement of the tracer particle velocity by EP while the flow was still at rest), and good agreement was found.

An alternative optical method to quantify the electrophoretic and electroosmotic mobilities is based on the Particle Tracking Velocimetry (PTV) technique [20]. Oddy and Santiago [20] imposed forcings through alternating current (AC) and DC electric fields; the resulting particle displacement, when those flows are fully-established, were measured and used to determine the mobilities from the solution of

two second order algebraic equations. Their method requires the use of two custom programs, one associated with AC and another with DC, to determine, respectively, the streak lengths and the particle displacements. A statistical analysis was also used to obtain the mobility distributions based on the measured particle displacements of several particles.

The aim of the present study is to further explore the different time responses of TP to EO and EP induced motion, either under constant (DC) or periodic (AC) imposed electric fields, and to present two different methods to quantify the channel walls and TP zeta-potentials. The two methods are here coined as the pulse method and the sine-wave method, and they extend existing techniques, which invariably have been developed for Newtonian fluids. In the pulse method here described, in the same experiment both the EP and EO velocities can be measured directly in one single run (electric pulse startup measures EP velocity and pulse shutdown measures EO velocity), contrasting with earlier methods [13, 14] in which the EP velocity is directly measured, but then the EO velocity is obtained indirectly as the difference between the particle velocity and the EP velocity after the EO flow is established. Additionally, we use the pulse method to test the complex dynamic response of viscoelastic fluids in the flow startup and shutdown. Regarding the sine-wave method, it shares some similarities with other published methods (*e.g.* [15, 20]), in the sense that they share some optical techniques, equations or general underlying principles, but they differ in the way the physical parameters are measured and consequently they are different methods, each having distinct advantages and drawbacks. As referred to above, Oddy and Santiago [20] also used PTV but relied on a combination of two complementary DC and AC forcing experiments, whereas here only a single AC experiment is required to obtain both the EP and EO mobilities. In addition, our determination of both mobilities in the sine-wave method also relies on a minimization of error between experimental data and an analytical solution, but otherwise the optical technique and the flow is quite different from the steady flow used by Yan et al. [15].

In this work, the experimental velocities are measured using the PTV technique, due to its high temporal resolution capability.

The pulse and sine-wave methods are described in the next section, together with the theoretical background and the experimental set-up used. In Section 3, the two methods are compared using Newtonian fluids. For the pulse method, the flow behavior using non-Newtonian (viscoelastic) fluids is also analyzed, to show the applicability of this method to complex fluids. The paper ends with the main conclusions from this work.

2 Materials and methods

2.1 Theory and governing equations

Consider a straight microchannel filled with an electrolyte containing neutrally-buoyant tracer particles, where an electric field is applied without any external pressure gradient imposed. In steady-state conditions, the TP velocity (observed velocity, u_{obs}) results from multiple contributions:

$$u_{obs} = u_{eo} + u_{ep} + u_{Bm} \tag{1}$$

where u_{eo}, u_{ep} and u_{Bm} are the EO, EP and Brownian motion velocities, respectively. In the present work, Brownian motion can be neglected relative to the other two terms (after averaging the values among several particles the random motion component cancels out).

A simple, yet realistic, expression for u_{eo} can be derived from the Helmholtz-Smoluchowski theory for Newtonian fluids [16, 20]:

$$u_{eo} = -\frac{\varepsilon \zeta_w}{\mu} E \tag{2}$$

where ζ_w is the wall zeta-potential, E is the applied electric field, and ε and μ are respectively the electric permittivity and shear viscosity of the solution. Equation (2) is valid for $\lambda_D << L$, where λ_D is the Debye length (quantifying the EDL width) and L is the channel characteristic length scale.

The EP velocity can be expressed in a similar way (after simplifying Henry's equation [16, 20]), valid for Newtonian fluids:

$$u_{ep} = \frac{\varepsilon \zeta_p}{\mu} E \tag{3}$$

where ζ_p is the TP zeta-potential. A major difference between Eqs. (2) and (3) relies on the velocity direction: for the same applied electrical field and if both ζ_w and ζ_p have the same sign, the EP and the EO velocities have opposite signs. From a dynamic perspective, EP and EO typically have very different time-scales, when considering TP at the central region of the channel. For EO, the diffusion time-scale, τ_{eo}, is of the order [21]:

$$\tau_{eo} = O\left(\frac{\rho r_h^2}{\mu}\right) \tag{4}$$

where ρ is the electrolyte density and $r_h = wh/(w+h)$ is the channel hydraulic radius, which is the characteristic length scale of viscous diffusion, with w and h representing the width and depth of the microchannel, respectively. On the other hand, for EP the characteristic inertial time-scale, τ_{ep}, is of the order [20, 21]:

$$\tau_{ep} = O\left(\frac{\rho_p a^2}{\mu}\right) \tag{5}$$

where ρ_p and a are the particle density and radius, respectively. Comparing Eqs. (4) and (5), we conclude that for typical microfluidic devices and tracer particles, EP can be orders of magnitude faster than EO to become fully-developed. For example, for water with micro-particles of $a = O(10^{-6}$ m) placed in a microchannel with $r_h = O(10^{-4}$ m), time-scales τ_{eo} and τ_{ep} are of the order of 10 ms and 1 μs, respectively.

In addition to the two previous time-scales, two other values should be considered, which are related to the double layer polarization and concentration polarization. Both events refer to the ionic equilibrium that should be recovered in the

bulk after the ions migration to the channel/TP EDL. The characteristic time-scales for such phenomena are [20, 21]:

$$\tau_{dl} = O\left(\frac{\lambda_D^2}{D}\right) \text{ and, } \tau_{cp} = O\left(\frac{a^2}{D}\right) \quad (6)$$

where τ_{dl} is the double-layer polarization time-scale, τ_{cp} is the concentration polarization time-scale and D is the diffusion coefficient of the ions. Considering an electric double-layer with $\lambda_D = O(10^{-8}$ m) and a typical ion diffusivity in water $D = O(10^{-9}$ m^2/s), then τ_{dl} and τ_{cp} are of order 0.1 μs and 1 ms, respectively.

2.1.1 Pulse method

The pulse method considers the flow startup and flow shutdown when an electric pulse of constant amplitude is applied and subsequently removed. Due to the different time-scales of EP and EO, in the flow startup the particles will almost instantaneously start moving by EP, while the EO contribution at the center of the channel will increase progressively with time, until the steady-state velocity is reached over a time-scale of the order of τ_{eo}. Similarly, once the electric field is switched off, the EP velocity component vanishes almost instantaneously (within τ_{ep}), while the EO velocity component at the center of the channel will decay slowly, over the channel diffusion time-scale, τ_{eo}. These different startup and shutdown behaviors can be captured with a high-speed camera synchronized with the applied electric field. Using this approach, the characteristic velocities of electrophoresis and electroosmosis can be measured independently in a single realization of one experiment.

The distinguishing points of our method relative to previous works (*e.g.* [13, 16]) are: (1) in this work the TP velocity is measured by the PTV technique, instead of the commonly used micro-PIV; (2) a pulsed electric field is imposed, instead of a step signal, which allows exploring also the flow shutdown features (where we can again isolate EO from EP). It is worth noting that the PTV technique used here allows the analysis of each individual tracer particle, which can be advantageous, for example, when a mixture of different TPs is being analyzed in a single experiment, or a significant number of particles is analyzed to determine the distribution of their EP mobilities, as also done by Oddy and Santiago [20].

2.1.2 Sine-wave method

In the pulse method, EO and EP mobilities (and the corresponding zeta-potentials) can be directly computed from the experimental tracking of the pathlines of individual tracer particles, whereas the second method presented in this work strongly relies on the manipulation of more complex analytical expressions, as will be described in what follows.

The sine-wave method is based on the delay that occurs between an imposed sinusoidal electric field and the EO velocity response at the center of a straight channel, as well as on the delay between EO and EP velocity components. When an oscillatory electric signal is applied, the EO response of the fluid within the EDL is nearly instantaneous, but outside this region, the EO velocity will lag the imposed signal by the finite diffusion time-scale corresponding to the distance between the actual position and the wall. In addition, the maximum value of the EO velocity at the channel centerline will depend on the signal frequency [22]. When the period of the applied sinusoidal signal (T) is significantly higher than the characteristic time-scales associated with the particle (τ_{ep}, τ_{cp} and τ_{dl}), then it can be assumed that the EP velocity component is in phase with the imposed signal and its magnitude is independent of the imposed electric field frequency. In such conditions, the observed TP velocity (u_{obs}) results from the summation of one out-of-phase component (EO) with one in-phase component (EP). In a mathematical form, for an imposed electric field $E\sin(\omega t)$, with amplitude E and angular frequency $\omega = 2\pi f$, the observed TP velocity (u_{obs}) is given by:

$$u_{obs} = u_{ep}\sin(\omega t) + u_{eo}\beta(f)\sin(\omega t + \alpha(f)) \quad (7)$$

where $\beta(f)$ is a known frequency-dependent coefficient ranging from 0 to 1 for Newtonian fluids, $\alpha(f)$ is a known frequency-dependent delay of the EO velocity component relative to the imposed signal and u_{eo} and u_{ep} are the steady-state electroosmotic and electrophoretic velocities for a constant electrical field E, which for Newtonian fluids are given by Eqs. (2) and (3), respectively.

Marcos et al. [22] derived an analytical expression for the EO velocity of Newtonian fluids in a straight rectangular channel subjected to an oscillatory electric field, under the Debye-Hückel approximation (see Appendix A). This dimensionless velocity profile corresponds to the second term on the right-hand side of Eq. (7) after division by u_{eo} (considering u_{eo} from Eq. (2)) and it is independent of the zeta-potential, which is usually unknown. In practice, the dimensionless velocity profile is dependent on fluid properties (density, viscosity, dielectric permittivity and ionic concentration), on geometric factors (channel depth and width), on the applied signal properties (electric field magnitude and frequency) and on ambient variables (temperature). Therefore, only two unknowns remain in Eq. (7), the velocities u_{eo} and u_{ep}.

The procedure used in this work to estimate u_{eo} and u_{ep} is based on minimizing the sum of the square of difference between the observed TP velocity (u_{obs}) and the values computed from Eq. (7), for different frequencies. The following cost function (c) was used with u_{eo} and u_{ep} as design variables:

$$c = \sum_{i=1}^{n}\left[\sum_{j=1}^{m}\left[u_{obs}(t_j) - u_{ep}\sin(\omega_i t_j) - u_{eo}\beta(f_i)\right.\right.$$
$$\left.\left.\sin(\omega_i t_j + \alpha(f_i))\right]^2\right] \quad (8)$$

Note that Eq. (8) has a double summation. In the inner summation, each experimental velocity at time t is subtracted to the theoretical velocity expected at this same time, where

$t_1 = 0$ and $t_m = T_i$ (m is the number of acquired images in one signal period). This subtraction is performed over one signal period, for a given (fixed) signal frequency. The outer summation i varies over all the n tested frequencies (f_i), since the u_{eo} and u_{ep} variables are independent of the applied signal frequency.

The optimal solution to the minimization problem defined by Eq. (8) is found using the Matlab® (MathWorks, www.mathworks.com/) built-in *fminsearch* function, which is an implementation of the Nelder-Mead simplex algorithm [23].

The method robustness was assessed with artificial signals: the EO component was computed from the analytical expression in Appendix A and the EP component was assumed to be a sine function – the first term on the right hand side of Eq. (7), in phase with the applied electric potential. A Gaussian noise component was added to the artificial signals and several (u_{eo}, u_{ep}) pairs were tested (each value was multiplied by the corresponding component), with EP and EO having either the same or opposite signs. The algorithm was able to yield back the original values of (u_{eo}, u_{ep}) with an error that depended on the noise amplitude relative to the velocity magnitudes, but which was always below 5%, for a noise component as high as 50% of max ($|u_{eo}|$, $|u_{ep}|$). The optimal solution found by the algorithm was nearly insensitive to the initial guess of (u_{eo}, u_{ep}), over a wide range of values. Even though we used several different frequencies in our tests, we observed that using a single frequency in the summation of Eq. (8) was enough to extract accurate values of u_{eo} and u_{ep} provided the delay $\alpha(f)$ in Eq. (7) was high enough to avoid multiple solutions to the problem (in the limit of $\alpha(f) \to 0$, the two terms on the right-hand side become a single one and multiple solutions of (u_{eo}, u_{ep}) are possible).

The proposed method differs from previous methods (*e.g.* [15, 20]) in the following ways: (i) both the EP and EO mobilities (or zeta-potential values) can be determined in the same experiment in one single run, while previous methods usually required two different experimental conditions (one per each unknown); (ii) instead of solving a direct algebraic system of equations, we solve a single minimization problem.

2.2 Microchannel fabrication

The microchannels used in this work were fabricated using standard photolithography techniques. The SU-8 molds were used for casting in polydimethylsiloxane (PDMS; Sylgard 184, Dow Corning Inc). A 5:1 (wt/wt) PDMS:curing agent ratio was used in the fabrication process and the channels were left to cure overnight in an oven at temperature $T_{abs} = 353$ K. In order to ensure the same zeta-potential at all walls of the microchannel, all the four walls were made of PDMS. For that purpose, the glass slide used to seal the PDMS channels was covered with a thin PDMS layer, prior to sealing. The channels, schematically shown in Fig. 1, are 8 mm (channels A and B) and 16 mm (channel C) long (length l), with a rectangular cross-section (w x h) of 399 μm x 174 μm (channel A), 404 μm x 108 μm (channel B), and 404 μm x 178 μm (channel C).

In order to avoid the possible build-up of a streamwise pressure gradient, the two reservoirs located at each end of the microchannel were externally connected. With this system, the fluid displaced by EO is externally replenished and it is possible to run the device for a long time, without generating external pressure effects (nevertheless, Joule heating and electrode polarization can become an issue of concern in such case). A platinum electrode is immersed at each reservoir to impose the pulse or the sinusoidal electrical field.

To clean the surface of the microchannel walls before each experiment, the microchannel was sequentially washed with 10 mL of distilled water, followed by 10 mL of sodium hydroxide (10 mM), 10 mL of distilled water and finally 10 mL of the working solution.

2.3 Working fluids

A 1mM borate buffer (Sigma - Aldrich) was used as the standard working solution in this work. To test the concentration effect on the zeta-potential, 5 and 10 mM borate buffers were also used. In order to minimize the adhesion of particles to the walls, 0.05% (wt/wt) of sodiumdodecylsulfate (SDS, Sigma-Aldrich) was added to the buffer solutions, unless otherwise stated. The conductivity (measured with a CDB-387 conductivity meter) and the pH (measured with a pH 1000L, pHenomenal®, VWR probe/device) of the working solutions were measured after surfactant addition (see Table 1). In addition, the remaining properties of the solution are: density and viscosity, $\rho = 998$ kg/m^3 and $\mu = 0.955$ mPa.s, respectively, both at the temperature of the experiments, $T_{abs} = 295$ K; dielectric permittivity, $\varepsilon = 7.03\times10^{-10}$ C/Vm; ionic concentrations, $C = 1$, 5 and 10 mM.

The working solutions were seeded with 2 μm fluorescent polystyrene particles (FluoSpheres® Carboxylate-Modified Microspheres, Nile Red, $\rho = 1055$ kg/m^3, Molecular Probes®) at a weight concentration of 80 ppm (wt/wt). The surface of the particles is modified with carboxyl groups (−COOH), which, at the working pH, are deprotonated, presenting a negative charge.

Viscoelastic solutions were also used to examine the flow behavior by means of the pulse method, for non-Newtonian fluids. Aqueous solutions with 100, 200, and 400 ppm (wt/wt) of polyacrylamide (PAA, Polysciences) with high molecular weight, $M_w = 18 \times 10^6$ g mol^{-1}, were used. The polymer was directly dissolved in distilled water and no buffer was used, since this would decrease significantly the relaxation time, and consequently the elasticity of the fluid [24]. No surfactant was added to reduce particle adhesion to the walls, since the higher viscosity of the PAA solutions leads to negligible particle sedimentation. A rotational rheometer (Physica MCR301, Anton Paar) with a 75 mm cone-plate system with 1° angle was used to measure the shear-thinning viscosity of the solutions in steady shear flow, which is plotted in Fig. 2. The fluid relaxation time λ was also

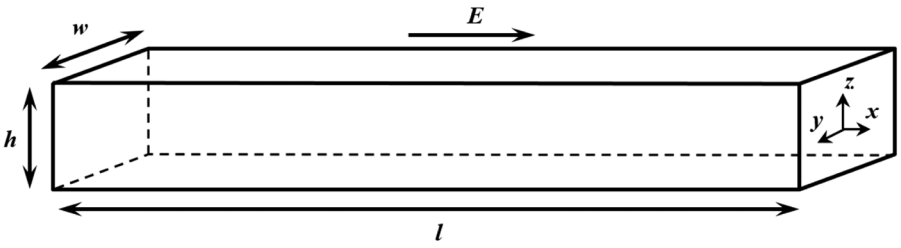

Figure 1. Schematic representation of the rectangular microchannel, its orientation relative to the imposed electric field and coordinate system.

Table 1. Electrical conductivity and pH of the working solutions (measured at $T_{abs} = 298$ K)

	Borate buffer			Polyacrylamide solution		
Concentration	1.0 mM	5.0 mM	10.0 mM	100 ppm (wt/wt)	200 ppm (wt/wt)	400 ppm (wt/wt)
pH	8.89	9.08	9.10	7.91	8.19	8.26
Electrical conductivity (μS/cm)	196	448	737	32.5	57.4	102.9

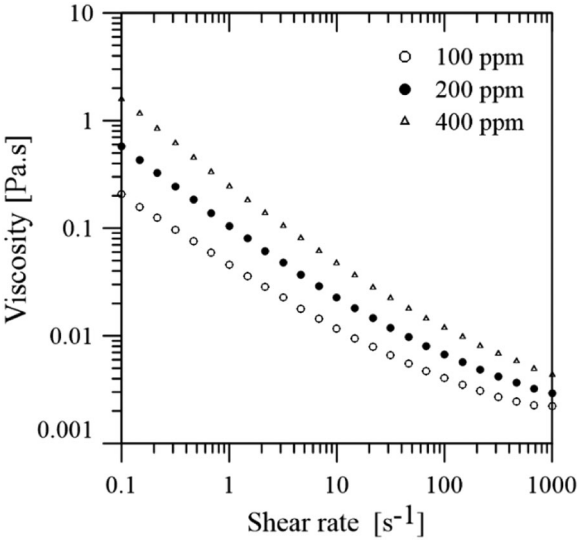

Figure 2. Influence of shear rate on the steady shear viscosity of the aqueous polyacrylamide solutions at $T_{abs} = 295$ K.

measured using a capillary-breakup extensional rheometer (Haake CaBER-1, Thermo Haake GmbH) and the values obtained were $\lambda = 0.018$ s, 0.060 s and 0.115 s for the 100 ppm, 200 ppm and 400 ppm aqueous PAA solutions respectively, all measured at $T_{abs} = 295$ K. The pH and conductivity were also measured for the solutions and are listed in Table 1.

2.4 Experimental set-up and PTV

The experimental set-up is represented schematically in Fig. 3. The electric field is imposed using a function generator (AFG3000 Series, Tektronix) connected to a high-voltage power amplifier (Trek, Model 2220). The function generator is simultaneously used to trigger the high-speed camera (Photron FASTCAM Mini UX100), in order to guarantee that the imaging system is synchronized with the electrical system. The high-speed camera captures the images from an inverted epi-fluorescence microscope (Leica Microsystems GmbH, DMI 5000M) equipped with a 20× objective lens (Leica Microsystems GmbH, numerical aperture $NA = 0.4$), a filter cube (Semrock CY3-4040C) and a continuous light source (100 W mercury lamp). In these conditions and using the camera full-resolution (1280 × 1024 pixels), each pixel was 0.498 μm × 0.498 μm. Unless otherwise stated, the camera acquired the images at 4000 frames per second (fps).

The PTV algorithm starts with an initial image processing step, where the tracer particles are identified by standard blob analysis. Briefly, particles are recognized based on intensity thresholding and their positions are computed with subpixel resolution. Since the number of particles tracked in each image was low, the frame rate was high and the flow was smooth, particle tracking simply relied on particle matching between frames, based on a minimal distance criterion. This image processing step can be either performed on commercial software packages, such as Matlab® (MathWorks, www.mathworks.com/), or in open-source packages, such as Blender (www.blender.org/) or ImageJ (www.imagej.net/). For the sake of simplicity, Matlab® (version R2012a) was used in all the image processing and numerical calculations reported here.

3 Results and discussion

3.1 Time-scale analysis

The validity of using the two methods is dependent on the relation between the different time-scales previously discussed in Section 2.1. For the experimental conditions of this work,

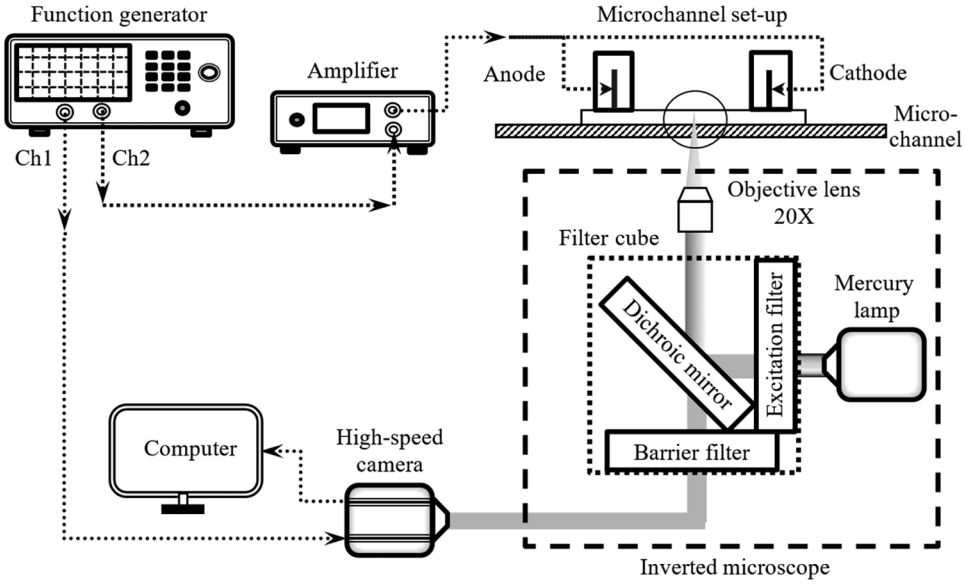

Figure 3. Diagram of the experimental set-up.

we have $\tau_{ep} = O(10^{-6}$ s), $\tau_{eo} = O(10^{-2}$ s), $\tau_{cp} = O(10^{-3}$ s) and $\tau_{dl} = O(10^{-7}$ s). For the pulse method to work adequately, max{τ_{ep}, τ_{cp}, τ_{dl}} and τ_{eo} should be clearly apart from each other, preferably by orders of magnitude. From the group of time-scales which will dictate a steady electrophoretic motion (τ_{ep}, τ_{cp}, τ_{dl}), we observe that τ_{cp} is only one order of magnitude lower than τ_{eo} and this should be taken into account when further analyzing the results. Indeed, at 4000 frames per second, the first frame is taken at $t = 2.5 \times 10^{-4}$ ms, which is lower than τ_{cp}, so that EP eventually is not yet fully-developed in the first few frames. For the sine-wave method, the smallest period of oscillation was $O(10^{-2})$ s, which is of the order of τ_{eo}, but higher than the remaining time-scales (those events can be assumed in equilibrium for oscillatory flow). As the signal period approaches τ_{eo}, the delay between the EO velocity component and the signal increases, a behavior that is well captured by Eq. (A1) (see appendix), thus not being problematic for the analysis (only care has to be taken with the first cycles which are not yet in the periodic regime and should be excluded).

3.2 Pulse method evaluation

Figure 4 presents the results obtained for an imposed electric field pulse from 0 to 440 V/cm using channel A ($h = 174$ μm). For averaging purposes, a continuous sequence of pulses was generated over all the camera recording time. Three pulse lengths were tested: 2, 8 and 40 ms, in individual runs of the same experiment. The time interval between consecutive pulses of the sequence was ten times larger, i.e. 20, 80, and 400 ms, respectively, to allow complete velocity decay between applied pulses. For data analysis, we take the average of the velocity among all the pulses for the same particle and then average over all the particles tracked (the results presented include an average of at least 20 particles). Only particles near the centerline were considered (within a deviation of ± 5% of the channel width in the planar spanwise direction; in depth, we are conditioned by the objective depth of field).

From Eq. (4), we estimate the diffusion time-scale of channel A as $\tau_{eo} \approx 15$ ms for the buffer solutions, thus only the pulse duration of 40 ms allows the full development of EO, as can be confirmed in Fig. 4. For this reason, the discussion presented next refers only to this longer pulse.

Four different regimes can be identified in the profiles of Fig. 4, which are illustrated in Fig. 5. The first regime (R_1) is dominated by EP, since the EO velocity boundary layer propagating from the channel walls still did not reach the channel centerline. This regime has a short duration and it is difficult to capture with a negligible EO contribution unless a very high acquisition rate is used. Furthermore, if we assume that EP is fully-developed and there is still no significant contribution from EO, a constant velocity would be expected, as illustrated in Fig. 5. However, we observe experimentally (Fig. 4) that the velocity in the first two to three captured frames is still decreasing, which can be a consequence of the non-negligible τ_{cp} time-scale. In the second regime (R_2), the EO component is developing, until it reaches its steady-state (for $t > \tau_{eo}$) in regime R_3. Since both the particles and the channel walls have a negative charge, EP and EO act on opposite directions (here $u_{ep} < 0$ and $u_{eo} > 0$), such that the TP invert their motion direction during regime R_2 (this happens because $|u_{eo}| > |u_{ep}|$). When the applied electric field pulse is stopped, the EP component *instantaneously* vanishes (within a time-scale $\tau_{ep} \approx 10^{-6}$ s) and the EO component becomes evident by a sharp increase in the velocity profile of Fig. 4B (beginning of regime R_4). The peak velocity will then decay to zero within a time-scale τ_{eo} similar to that observed for regimes $R_1 + R_2$, since no electric field is applied and because there is no pressure build-up in the channel. A natural consequence of this interpretation should be that the sum of the observed peak velocity in regime R_1 (−2.9 mm/s), with the peak velocity in

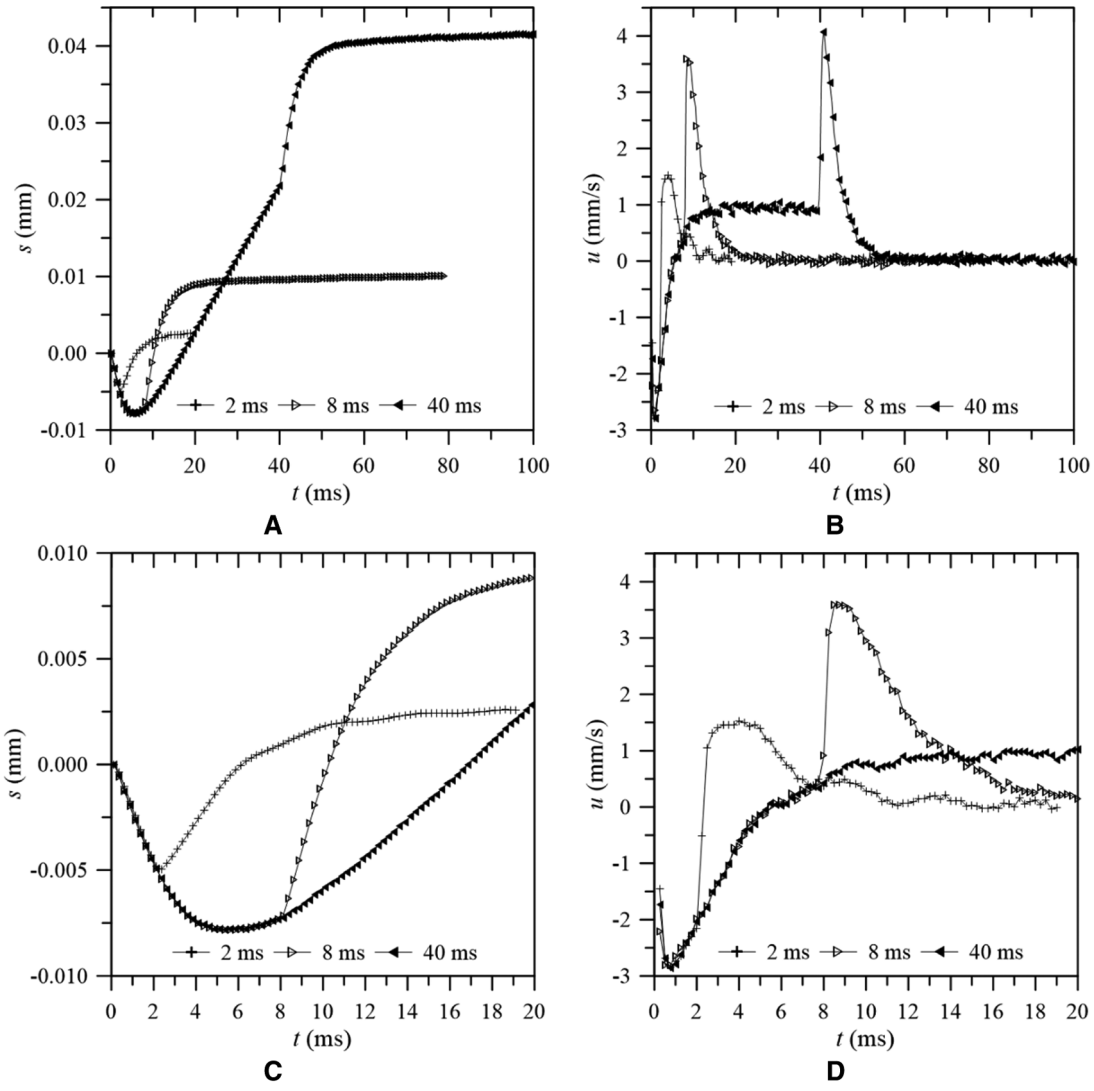

Figure 4. Tracer particle displacement s (A) and velocity u (B) at the centerline of channel A ($h = 174$ μm), for three applied electric pulse durations (2, 8, and 40 ms) with an amplitude of 440 V/cm. Plots (C) and (D) are a zoomed view of (A) and (B), respectively, at short times. The points represent average experimental values, while the lines are only a guide to the eye.

regime R_4 (4.1 mm/s) should be equal to the observed velocity in regime R_3 (1.0 mm/s). A difference of 20% is found between both values. The error can be attributed to a limited time-resolution to capture, both the electroosmotic-free velocity (u_{ep}) at the beginning of the experiments (R_1), as well as the sharp velocity peak due to electroosmosis in R_4, noting that both values result from an approximate finite-differences derivative computed at a single point. Nevertheless, further increasing the frame rate would lead to a light intensity reduction and this would require a change of the light source in our experiments. In addition, the TP displacement between frames would decrease and the noise in the computation of the velocity from the derivative of the particle position as a function of time would increase, although these effects could be compensated using a higher magnification objective. A better strategy would be a fitting procedure, similar to the sine-wave method, using the analytical expression given in Appendix A for a continuous signal. Also, the potential role of τ_{cp} in determining u_{ep} cannot be disregarded (this source of error can be minimized using smaller particles, which will reduce τ_{cp}).

The same method was repeated using the 108 μm deep channel B (Fig. 6), which has a lower diffusion time-scale ($\tau_{eo} \approx 8$ ms). The same four regimes were observed, with the only difference that EO now takes less time to develop and to decay. As can be seen in Fig. 6, both the pulse lengths of 8 and 40 ms allow the full development of the EO velocity component. The measured velocities in R_1, R_4 (at the beginning) and R_3 are −2.3, 3.7, and 0.9 mm/s, respectively.

In conclusion, our results suggest no significant variation in the determination of EP and EO velocities with the change in the channel dimensions, as expected, with small

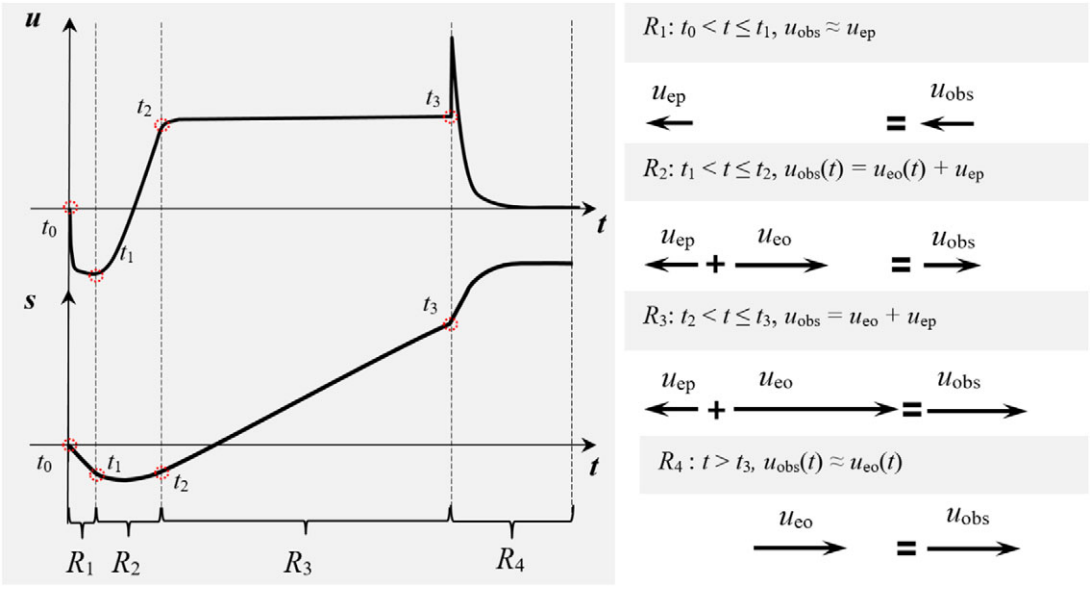

Figure 5. Regimes in the TP velocity u and displacement s profiles, at the channel centerline, for an electric pulse with a duration significantly higher than τ_{eo}, for channel/TP walls with equal polarity zeta-potential ($|\zeta_{eo}| > |\zeta_{ep}|$). In regime R_1, EP is fully-developed, while the EO boundary layer still has not reached the channel centerline. This is followed by regime R_2, where the EO component is developing and the overall velocity is consequently increasing with time. After the EO velocity component becomes fully-developed, regime R_3 starts, which is characterized by a constant velocity. The last regime (R_4) starts after the pulse ends and it is characterized by the EO velocity decay, since it is assumed that the EP component vanishes very quickly. It is also for this reason that an abrupt increase in the TP velocity is observed at the beginning of R_4 – the peak velocity corresponds to the EO velocity component. Adding the velocity in regime R_1 (u_{ep}) to the peak velocity of R_4 (u_{eo}) provides the combined velocity in regime R_3 ($u_{eo} + u_{ep}$). The pulse electric field is active in the period $0 < t < t_3$ and $t_2 \approx \tau_{eo}$.

differences between the measurement in different channels arising from experimental error.

3.3 Sine-wave method evaluation

In the sine-wave method, a sinusoidal electric field with zero offset and peak amplitude of 440 V/cm was imposed in the same experiment for three different frequencies $f = 20$, 40 and 80 Hz. Similarly to the pulse method, the applied electric field was kept active during all the recording time of the high-speed camera. For each particle in the vicinity of the channel centerline, the first five cycles were neglected to avoid transient effects and the remaining cycles were averaged. Then, an average was performed on the velocities between different particles (at least 20 particles), in order to obtain a single average velocity profile for each frequency (however, the method can also be applied directly to the velocity profile of each particle). Note that using a fixed frame rate for all the frequencies results in a different number of points within one signal period for each frequency (lower frequencies will have a higher number of points per period). Since the inner summation of Eq. (8) is taken over all the points within one period, this would overweight the frequencies with a higher number of points. To avoid this issue, a sinusoid was fitted to the (velocity *vs* time) experimental profiles of each frequency and the resulting fit was always evaluated with the same number of points (typically 200 points within one period) regardless of the frequency. However, we should note that this fitting procedure is not essential for the process, since the weighting issue can be avoided in many different ways.

The results for channels A and B are presented in Fig. 7. The delay between the imposed electric signal and the TP velocity increases with the electric signal frequency due to the non-negligible delay of the development of the EO velocity component. Furthermore, this delay increases with the increase of the channel depth, since the momentum generated near the walls takes longer to diffuse toward the channel centerline. The best fit found by the applied algorithm is: $u_{eo} = 4.3$ mm/s and $u_{ep} = -3.5$ mm/s in channel A and $u_{eo} = 4.1$ mm/s and $u_{ep} = -3.2$ mm/s in channel B. This shows that the method yields similar results, with a difference below 10%, in channels with different dimensions.

In order to further validate the theory behind the method used, the analytical solution was evaluated over one period of time in the spanwise direction, using the best fit parameters. Although the optimized solution was obtained based on the dynamic velocity profiles at a fixed position (the centerline), the method is also able to predict the experimentally observed particle velocities in the spanwise direction at any time within a full period cycle. This is shown in Fig. 8 for different instants of time within a cycle (animations are provided as Supporting materials), and good agreement is always observed between

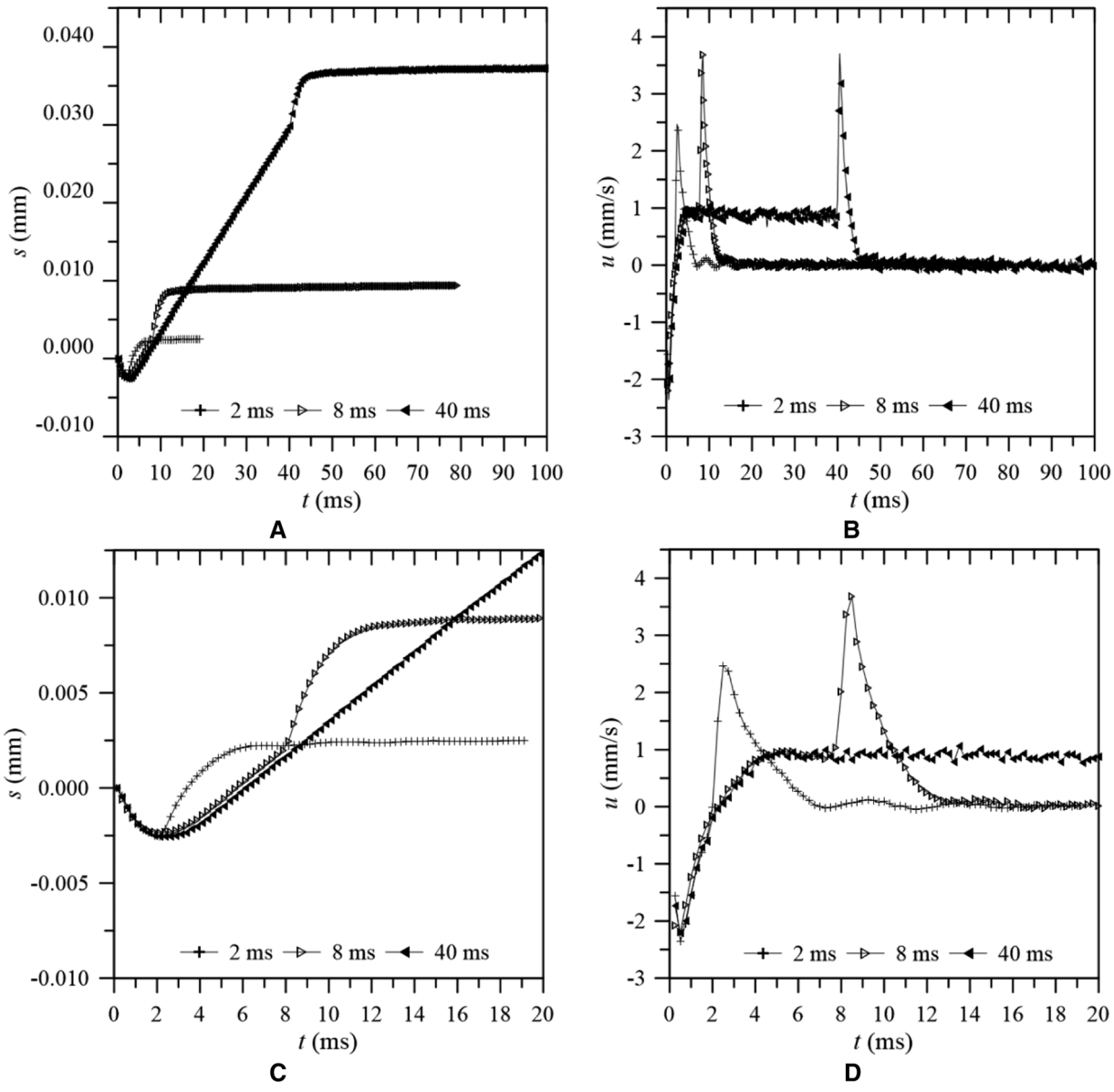

Figure 6. Tracer particle displacement s (A) and velocity u (B) at the centerline of channel B ($h = 108$ μm), for three applied pulse durations (2, 8, and 40 ms) with an amplitude of 440 V/cm. Plots (C) and (D) are a zoomed view of (A) and (B), respectively, at short times. The points represent average experimental values, while the lines are only a guide to the eye.

experimental data and the analytic solution. These results also suggest an alternative implementation of the sine-wave method: instead of using the velocity measured over time at a fixed position, the velocity profile measured at different spanwise coordinates and at a fixed time can be used.

3.4 Quantification of the zeta-potential of tracer particles and channel walls

In the previous section, the EO and EP velocities measured using the pulse and sine-wave methods were presented. In this section, those velocities are converted to values of zeta-potential.

The wall zeta-potentials can be computed using Eqs. (2) and (3), from the slopes of u-E curves, which are commonly known as the EP and EO mobilities. Those curves were obtained for both methods, in channels A and B, by changing the applied electric field magnitude, Fig. 9.

A first glance on Fig. 9 shows a good agreement between both methods, but better for the deeper channel, due to the temporal resolution constraint of the pulse method in channel B given its lower value of τ_{eo}, as previously discussed. Moreover, both EO and EP velocities are linear functions

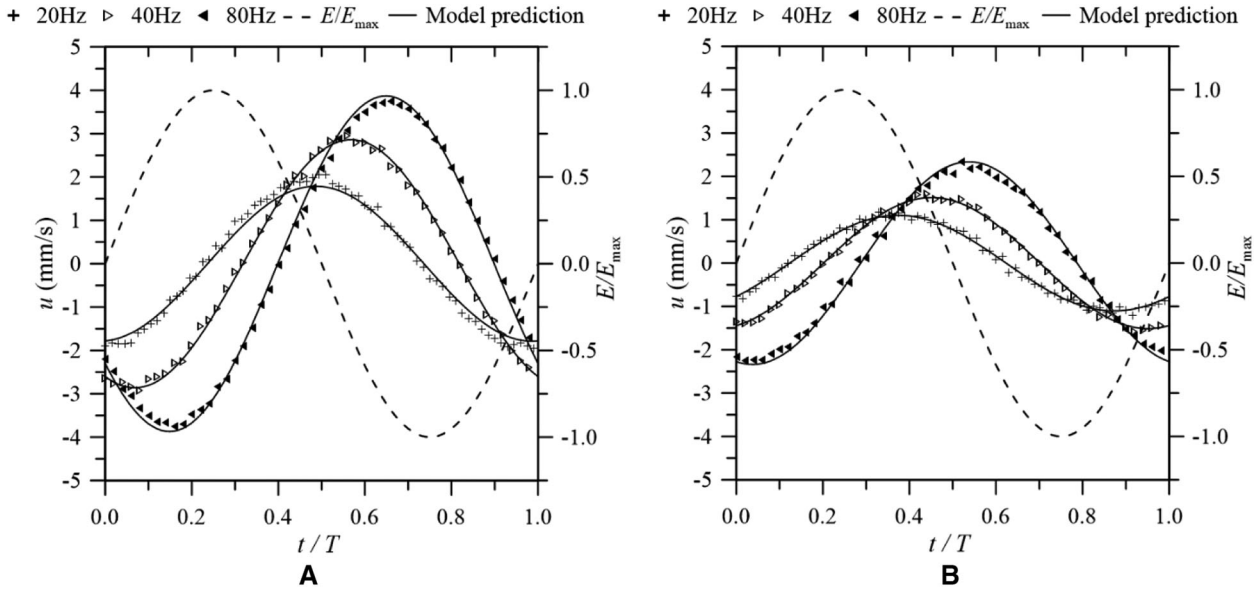

Figure 7. Tracer particle velocity u at the centerline of (A) channel A ($h = 174$ μm) and (B) channel B ($h = 108$ μm) under a sinusoidal electric field with a peak amplitude of 440 V/cm, for three different frequencies: $f = 20$, 40, and 80 Hz. The dashed line represents the dimensionless imposed electric signal, while the full lines represent the fitting of Eq. (7). The symbols are the average (over cycles and over particles) of experimental data. The best fit found by the algorithm for those conditions gives $u_{eo} = 4.3$ mm/s and $u_{ep} = -3.5$ mm/s for channel A and $u_{eo} = 4.1$ mm/s and $u_{ep} = -3.2$ mm/s for channel B.

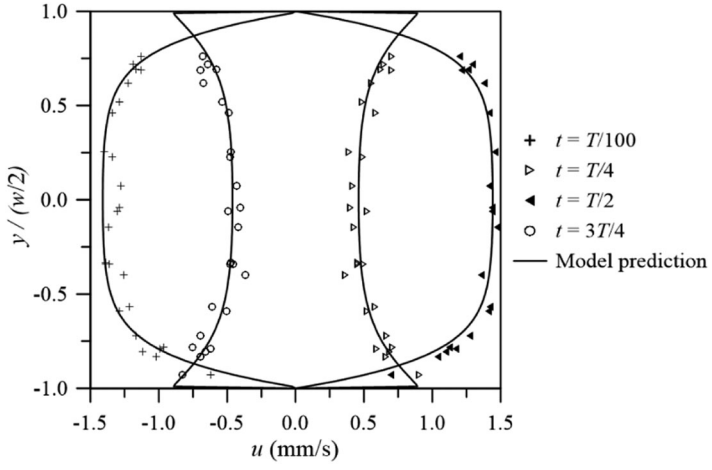

Figure 8. Spanwise profiles of TP velocity at four different instants of time within a cycle of period T for channel B ($h = 108$ μm) under forcing by a sinusoidal electric field with a peak amplitude of 440 V/cm, at $f = 40$ Hz. The points represent experimental averaged values over several cycles, while the lines represent the analytical prediction of Eq.(A1) using the best-fit parameters. The channel walls are located at $y/(w/2) = \pm 1$.

of the electric field magnitude, as expected theoretically for Newtonian fluids.

The estimated zeta-potentials are summarized in Table 2. Both the PDMS walls and tracer particles display negative values, as expected. However, our results are higher than other published values. For instance, Sze et al. [11] found zeta-potential values for PDMS surfaces varying between −110 and −68 mV for 10^{-4} M KCl, 10^{-3} M KCl and 10^{-3} M $LaCl_3$ electrolytes, and Ichiyanagi et al. [6] reported a PDMS wall zeta-potential of -74.4 ± 1.2 mV for 5 mM borate buffer (pH 9.4). Both these works report the use of buffers without addition of a surfactant. A plausible hypothesis for the observed differences could be the use of surfactant in our buffer solutions, which was seen to increase the EO mobility in previous studies [25, 26]. Also, a slight increase in the temperature (Joule heating, radiation heating by the mercury lamp, among others sources) would lead to a lower buffer viscosity, which was not taken into account in the calculations.

The results shown in Table 2 show good agreement between both techniques and for channels A and B, except for the lower value of the zeta-potential of the micro-particles measured in channel B. This discrepancy is a result of the smaller diffusion time-scale τ_{eo} in channel B, thus the EP

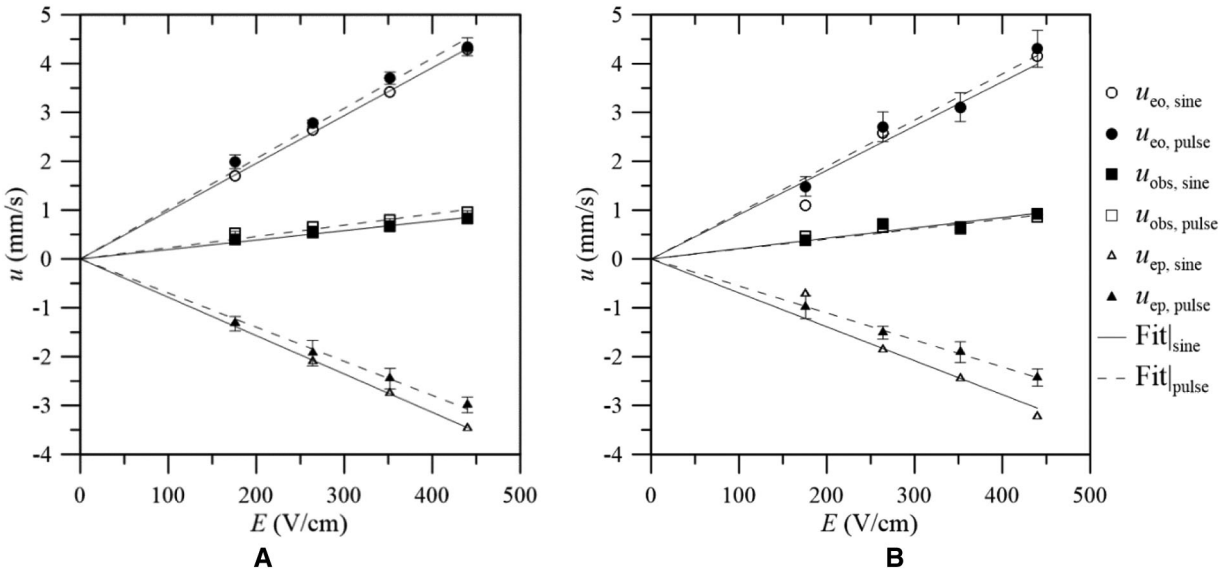

Figure 9. Tracer particle velocity components (EO, EP and OBS = EO+EP) as a function of the applied electric field magnitude, in (A) channel A ($h = 174$ μm) and (B) channel B ($h = 108$ μm). The EP/EO mobility is estimated from the slope of the linear fit to the corresponding points (dashed and full lines in the plot). Error bars represent the standard deviation for the pulse method (at least 20 particles were considered in each experiment). $u_{obs,pulse}$ is the combined (EO +EP) velocity in R_3 of Fig. 5, whereas $u_{obs,sine}$ represents the sum of the best-fit parameters ($u_{eo} + u_{ep}$).

Table 2. Wall zeta-potential of TP and PDMS microchannels for the 1.0 mM borate buffer with 0.05% SDS. The standard deviation is obtained from the 95% confidence interval for the slope of the linear fits in Fig. 9

	Zeta-potential of PDMS walls (mV)		Zeta-potential of TP (mV)	
	Sine-wave method	Pulse method	Sine-wave method	Pulse method
Channel A	-133 ± 3	-140 ± 11	-107 ± 3	-95 ± 6
Channel B	-123 ± 22	-129 ± 15	-94 ± 21	-75 ± 2

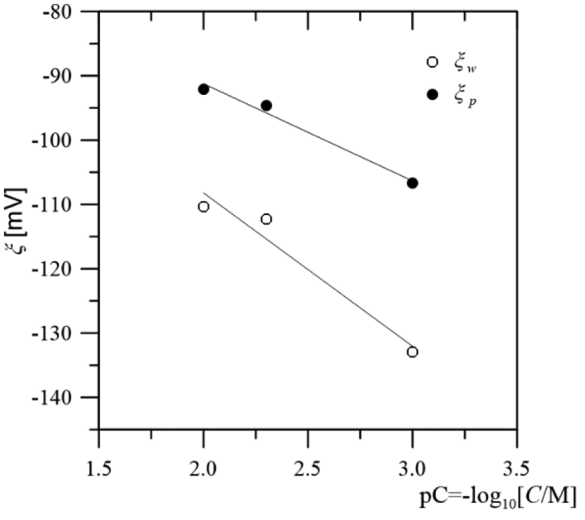

Figure 10. Wall zeta-potential dependence on the ionic concentration (pC) measured in channel A ($h = 174$ μm). The points represent experimental data, while the lines are linear fits.

velocity measured in the first frames already includes some influence of EO, leading to a decrease (in magnitude) of the estimated EP velocity. To minimize this discrepancy a higher acquisition rate is necessary.

To assess the influence of surfactant addition in the measured zeta-potentials, an additional test was performed without the addition of surfactant to the buffer solutions. The values obtained for the wall zeta-potentials of TP and PDMS, using the sine-wave method in channel A, were -85 ± 2 mV and -103 ± 2 mV, respectively for a borate buffer concentration of 1.0 mM. As expected, those values are lower (in magnitude) than the estimated zeta-potentials presented in Table 2, and similar to previous works.

3.5 Ionic concentration effect on the zeta-potential

The sine-wave method was also used to assess the conductivity effect on the wall zeta-potentials, using channel A. For the three ionic concentrations tested, a quasi-linear decrease (in a log-linear scale) of the zeta-potential is shown in Fig. 10,

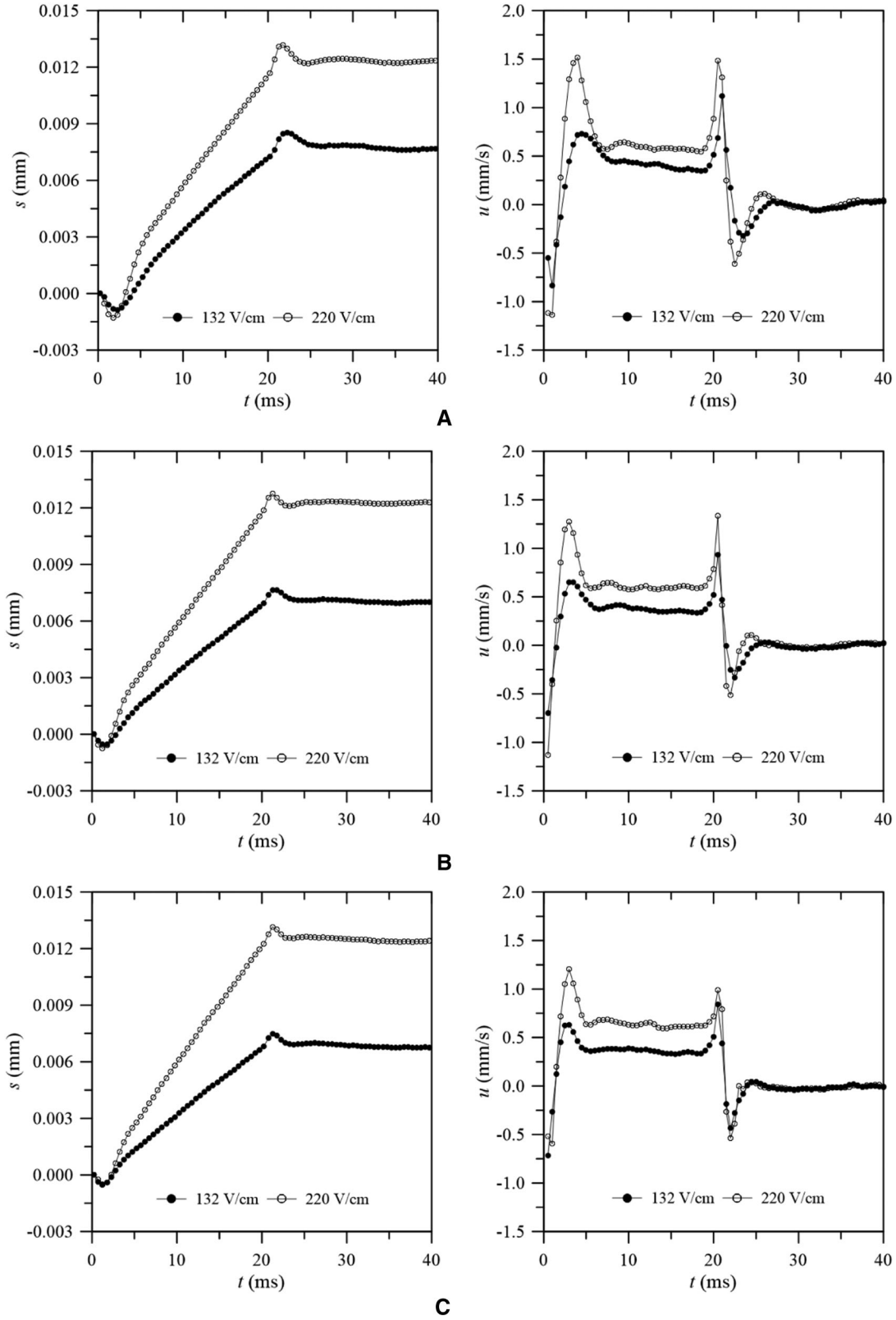

Figure 11. Tracer particle displacement (left hand-side), and velocity u (right hand-side) at the centerline of channel C ($h = 178$ μm), for an applied pulse duration of 20 ms with amplitudes of 132 and 220 V/cm, for polyacrylamide aqueous solutions at the following concentrations: (A) 100 ppm; (B) 200 ppm; (C) 400 ppm. The points represent average experimental values, while the lines are only a guide to the eye.

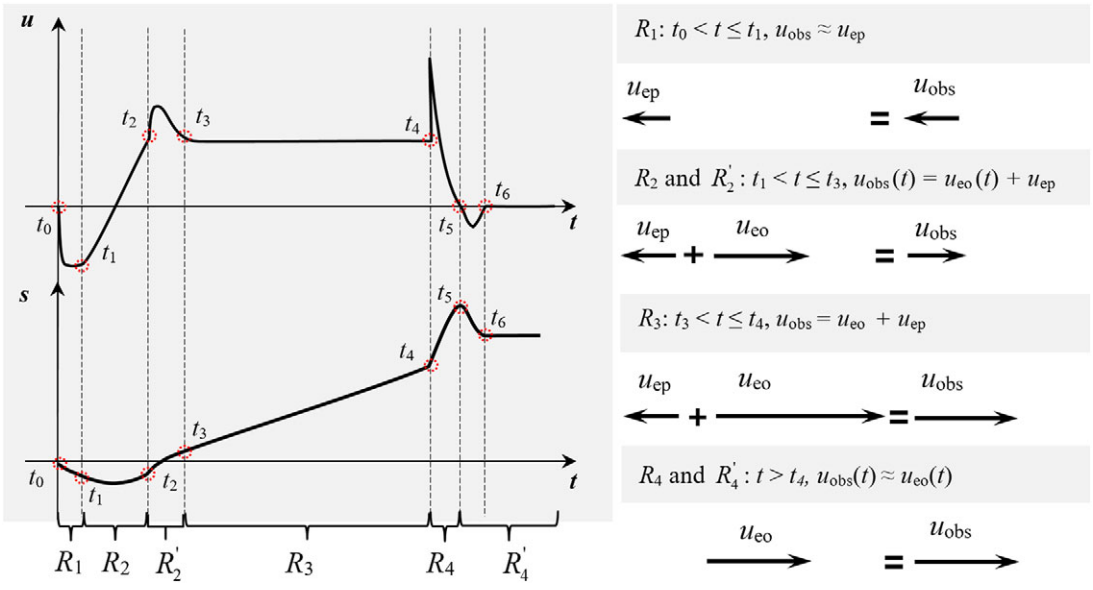

Figure 12. Regimes in the TP velocity u and displacement s profiles, at the channel centerline, for a viscoelastic fluid, due to an applied electric pulse. In regime R_1, EP dominates. This is followed by regime R_2, where the EO component is still developing to become fully-developed, but before achieving fully-developed flow condition, an overshoot (R_2') occurs and decays. Afterwards regime R_3 starts, which is characterized by a constant velocity. Regime R_4 starts after the pulse ends and is characterized by a zero EP component and before it decays completely, there is a velocity undershoot (R_4') followed by a decay to zero velocity.

when increasing the buffer concentration (conductivity). The slope of this linear relation for the PDMS walls (−24 mV/pC) is close to the published value of −29.75 mV/pC in Ref. 26.

3.6 Advantages and disadvantages of the pulse and sine-wave methods

The two methods illustrated in this work rely on the PTV technique to track the position of tracer particles and compute the corresponding velocity as function of time.

The pulse method shows a stronger dependence on the time resolution of the measurement system than the sine-wave method. In fact, it should be guaranteed that the first frame captured has a negligible contribution from EO in order to consider that it corresponds to the pure EP velocity (an alternative is to use Eq. (A1) to estimate the EO contribution at the first frame and include this correction in the calculation, or using Eq. (A1) to fit the velocity profile in regimes 1 and 2). For wider channels this criterion can be easily met with a low frame rate camera, but as the channel size decreases, a high-speed camera is required and may even be insufficient. On the other hand, the sine-wave method requires the occurrence of a delay between the applied electric signal and the EO response, which requires increasing the applied electric signal frequency as the channel dimensions decrease. Increasing the frequency further increases the required frame rate of the camera, which must be high enough to process an adequate number of data points within each periodic cycle. However, this dependence on the frame rate is not as strong as in the pulse method. For

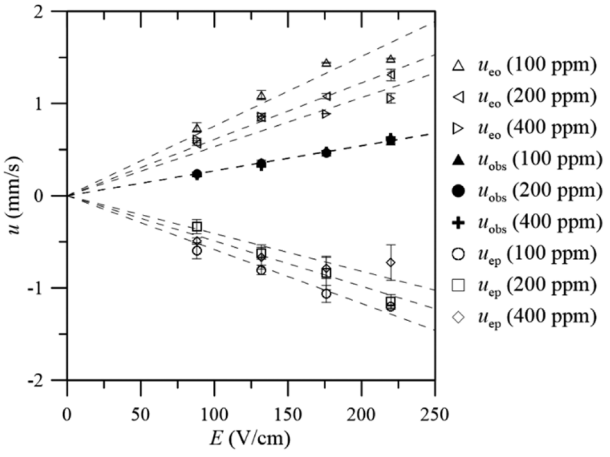

Figure 13. Tracer particle velocity components (EO, EP, and OBS = EO + EP) as a function of the applied electric field magnitude, in channel C (h = 178 μm) for PAA solutions with concentrations of 100, 200, and 400 ppm. The dashed lines are a guide to the eye. Error bars represent the standard deviation for the pulse method (at least 20 particles were considered in each experiment).

instance, the sine-wave method was tested with a frame rate of 400 fps, which is ten times lower than the frame rate typically used in this work and the velocities (u_{eo} and u_{ep}) found by the error minimization algorithm remained almost unchanged (in this test, the velocity profile had only five points in one periodic cycle at f = 80 Hz). Such low frame rate would give unacceptable results in the pulse method, since the first frame would correspond already to 35% of the

diffusion time-scale of channel B. Concluding, in respect to the time resolution requirements, the sine-wave method is more robust and less demanding in terms of the required acquisition rate. However, in channels with a high diffusion time-scale (large dimensions), both methods should perform acceptably.

From a practical perspective, the sine-wave method can be advantageous due to its weaker tendency to form bubbles at the electrodes (this only happens at low frequencies), even though both methods use the same electrodes. The test/processing time is also similar in both methods, but implementation of the sine-wave method can be more time consuming than for the pulse method. Actually, for the latter, a minimum effort is required if the particle tracking is performed with a software already prepared to automatically execute this task, such as the open source Blender, or ImageJ programs.

3.7 Response of viscoelastic fluids to an electric pulse

The previous sections described and assessed the transient response of Newtonian fluids to an electric field pulse during startup and shutdown. Due to the fading memory of viscoelastic fluids, which can be quantified by their relaxation time, it is relevant and interesting to investigate the response of a viscoelastic fluid to an applied electric pulse, since it is also desirable to measure its mobilities in the set-up. We tested polyacrylamide aqueous solutions at 100, 200, and 400 ppm weight concentrations subjected to a pulse length of 20 ms, which is longer than the estimated τ_{eo} for channel C (178 μm deep and 16 mm long). The results for step amplitudes of 132 and 220 V/cm are presented in Fig. 11. In this case, six different regimes can be identified and outlined, as shown in Fig. 12. Comparing with the Newtonian fluid response in Fig. 5, the overall behavior for viscoelastic fluid is similar, but additional velocity over- and under-shoots are present. Specifically, there are two additional regimes in the TP displacement and corresponding velocity profiles: overshoot (R_2') and undershoot (R_4') regimes, where fluid elasticity combined with the startup and shutdown transient was the key to the appearance of such two new regimes. Such overshoot/undershoot after positive/negative step variations of the applied electric field are a consequence of the memory of the fluid and the exponential decays observed in regimes R_2' and R_4' can be used to estimate the relaxation time of the fluid. Accordingly, due to that transient response, the pulse method will require future investigations.

Figure 13 shows the tracer particle velocity components (EO, EP and OBS = EO+EP) as a function of the applied electric field magnitude for the three aqueous polyacrylamide solutions, obtained from the velocity measurements illustrated in Fig. 11, and other not shown at different electric field strengths. The three velocities plotted were independently measured: the EP velocity is obtained from the minimum velocity at short times, the EO velocity corresponds to the peak velocity observed right after the electric field shutdown, and the combined velocity corresponds to the velocity plateau observed approximately between 5 and 20 ms. The results shown in Fig. 13 are similar to those obtained with the buffer solution, despite the significantly higher shear viscosities of the viscoelastic solutions. This observation should be a result of the shear thinning nature of the viscoelastic solutions, with the shear viscosity plateau at high shear rates approaching the shear viscosity of water (the local shear rates in the EDL are very large due to the locally high velocity gradients), or due to the formation of a near-wall layer depleted of macromolecules (see [27] for a theoretical analysis), which also explains the quasi-linear increase of the EO and EP velocities with the applied electric field strength. Future studies will be done with other polymer solutions to assess these hypotheses.

4 Concluding remarks

In the present work, we explored two methods that allow the simultaneous determination of the zeta-potential of tracer particles and channel walls in straight rectangular microchannels. In the pulse method, a pulse electric field is generated and the EP and EO velocities are determined based on the measurement of the variation with time of the particle velocity just after the pulse is turned on and off, respectively. This is possible due to the different characteristic time-scales of EO and EP. In the sine-wave method, a sinusoidal electric field with zero mean is imposed and the difference between the experimentally measured velocity of TP and the computed velocity using the analytical expression is minimized via an optimization procedure, where EO and EP velocities are the design variables. This method is based on the frequency-dependent delay between the EO and EP (or signal) velocity component responses. Both methods rely on the particle tracking velocimetry technique to measure the velocity of tracer particles. The pulse method is shown to be more dependent on a high time-resolution set-up than the sine-wave method, although it is of easier implementation. However, in channels with a high diffusion time-scale (large dimensions), both methods provide consistent results. In addition, the pulse method is easily extended to deal with non-Newtonian fluids, but that is not the case for the sine-wave method, unless the corresponding analytic solution is known, a non-trivial limitation for complex fluid rheology.

In the pulse method, Newtonian fluids show four regimes in the TP displacement and velocity profiles, while for viscoelastic fluids two additional regimes can appear, exhibiting an overshoot and an undershoot in the particle velocity response, which arise due to the fading memory of the viscoelastic fluid in combination to their response to electrical pulse startup and shutdown events.

S.H.S. acknowledges financial support from Fundação para a Ciência e a Tecnologia (FCT) [SFRH/BD/85971/2012]. F.P. and M.A.A. acknowledge funding from the European Research

Council (ERC) under the "Ideas" specific programme of the 7th framework programme (Grant agreement n. 307499).

The authors have declared no conflict of interest.

5 References

[1] Lewpiriyawong, N., Yang, C., Lam, Y. C., *Biomicrofluidics* 2008, *2*, 34105.

[2] Smoluchowski, M. V., *Handbuch Der Elektrizität Und Des Magnetismus*, Verlag von Johann Ambrosius Barth, Leipzig 1921, 379–387.

[3] Komagata, S., *Res. of the Electrotech. Lab. (Japan)* 1933, 8–13.

[4] Lane, T. B., White, P., *Phil. Mag.* 1973, *23*, 824–828.

[5] Mori, S., Okamoto, H., Hara, T., Aso, K., *Fine Particles Processing*, AIME 1980, Las Vegas, Nevada, 632–651.

[6] Ichiyanagi, M., Saiki, K., Sato, Y., Hishida, K., 12th International Symposium on Application of Laser Technology to Fluid Mechanics (Cd-Rom) 2004, paper 5.3, 1–11.

[7] Sato, Y., Hishida, K., *Fluid Dynam. Res.* 2006, *38*, 787–802.

[8] Tatsumi, K., Nishitani, K., Fukuda, K., Katsumoto, Y., Nakabe, K., *Measurement Sci. Technol.* 2010, *21*, 105402.

[9] Shin, S., Kang, I., Cho, Y.-K., *Colloids Surfaces a: Physicochem. Engineer. Aspects* 2007, *294*, 228–235.

[10] Ren, L., Escobedo-Canseco, C., Li, D., *J. Colloid. Interf. Sci.* 2002, *250*, 238–242.

[11] Sze, A., Erickson, D., Ren, L., Li, D., *J. Colloid. Interf. Sci.* 2003, *261*, 402–410.

[12] Huang, X., Gordon, M. J., Zare, R. N., *Analyt. Chem.* 1988, *60*, 1837–1838.

[13] Yan, D., Nguyen, N. T., Yang, C., Huang, X., *J. Chem. Phys.* 2006, *124*, 021103.

[14] Yan, D. G., Yang, C., Nguyen, N. T., Huang, X. Y., *Phys. Fluids* 2007, *19*, 017114.

[15] Yan, D., Yang, C., Nguyen, N. T., Huang, X., *Electrophoresis* 2006, *27*, 620–627.

[16] Sureda, M., Miller, A., Diez, F. J., *Electrophoresis* 2012, *33*, 2759–2768.

[17] Miller, A., Villegas, A., Diez, F. J., *Electrophoresis* 2015, *36*, 692–702.

[18] Bruus, H., *Theoretical Microfluidics*, Oxford University Press, Inc., New York 2008.

[19] Tabeling, P., *Introduction to Microfluidics*, Oxford University Press, Inc., New York 2005.

[20] Oddy, M. H., Santiago, J. G., *J Colloid Interf Sci* 2004, *269*, 192–204.

[21] Minor, M., van der Linde, A. J., van Leeuwen, H. P., Lyklema, J., *J. Colloid. Interf. Sci.* 1997, *189*, 370–375.

[22] Marcos, Yang, C., Wong, T. N., Ooi, K. T., *Internat. J. Engineer. Sci.* 2004, *42*, 1459–1481.

[23] Lagarias, J. C., Reeds, J. A., Wright, M. H., Wright, P. E., *SIAM J. Optimiz.* 1998, *9*, 112–147.

[24] Campo-Deaño, L., Galindo-Rosales, F. J., Pinho, F. T., Alves, M. A., Oliveira, M. S. N., *J. Non-Newtonian Fluid Mech.* 2011, *166*, 1286–1296.

[25] García, C. D., Dressen, B. M., Henderson, A., Henry, C. S., *Electrophoresis* 2005, *26*, 703–709.

[26] Kirby, B. J., Hasselbrink, E. F., Jr., *Electrophoresis* 2004, *25*, 203–213.

[27] Sousa, J. J., Afonso, A. M., Pinho, F. T., Alves, M. A., *Microfluid. Nanofluid.* 2011, *10*, 107–122.

Appendix A

Under the Debye-Hückel approximation, Marcos et al. [22] derived the following analytic expression for the EO velocity, $\bar{u}(\bar{y},\bar{z},\bar{t})$ (the overbars denote dimensionless values), in a straight rectangular channel subjected to an oscillatory electric field of the form $E(t) = Ee^{i\omega t}$:

$$\bar{u}(\bar{y},\bar{z},\bar{t}) = \frac{-64}{hw}\bar{G}\bar{E}\sum_{m=1}^{\infty}\sum_{n=1}^{\infty}C_{mn}\frac{e^{\left[\frac{i\omega D_h^2}{\upsilon}\bar{t}\right]}-e^{-\left[D_h^2\pi^2\left(\frac{(2m-1)^2}{w^2}+\frac{(2n-1)^2}{h^2}\right)\bar{t}\right]}}{\left[4\pi^2\left(\frac{(2m-1)^2}{w^2}+\frac{(2n-1)^2}{h^2}\right)+i\frac{4\omega}{\upsilon}\right]} \times \cos\left[(2m-1)\frac{D_h}{w}\pi\bar{y}\right]\cos\left[(2n-1)\frac{D_h}{h}\pi\bar{z}\right] \tag{A.1}$$

where

$$C_{mn} = \overline{\zeta_w}\frac{(-1)^{m+n}w}{(2m-1)\pi D_h\left(\frac{\left[1+(2m-1)^2\pi^2 D_h^2/\bar{\kappa}^2 w^2\right]\bar{\kappa}^2}{(2n-1)D_h\pi/h}+(2n-1)D_h\pi/h\right)} + \overline{\zeta_w}\frac{(-1)^{m+n}h}{(2n-1)\pi D_h\left(\frac{\left[1+(2n-1)^2\pi^2 D_h^2/\bar{\kappa}^2 h^2\right]\bar{\kappa}^2}{(2m-1)D_h\pi/w}+(2m-1)D_h\pi/w\right)} \tag{A.2}$$

with h and w representing the microchannel depth and width, respectively. The non-dimensional variables are $\bar{u} = u/u_{sh}$, $\bar{t} = \upsilon t/{D_h}^2$, $\bar{y} = y/D_h$, $\bar{z} = z/D_h$, $\bar{E} = ED_h\mathrm{Re}/\zeta_w$, $\bar{G} = 2z_v e n_0\zeta_w/\rho\,{u_{sh}}^2$, $\overline{\zeta_w} = z_v e\zeta_w/k_b T_{abs}$, $\bar{\kappa} = \kappa D_h$ and the Reynolds number, $\mathrm{Re} = \rho D_h u_{sh}/\mu$, where t is the time, T_{abs} is the absolute temperature, k_b is Boltzmann constant, κ is the Debye–Hückel parameter, $D_h = 2hw/(h+w)$ is the hydraulic diameter, $\upsilon = \mu/\rho$ is the fluid kinematic viscosity, ζ_w is the microchannel wall zeta-potential, u_{sh} is the Smoluchowski EO velocity, E is the electric field, z_v is the electrolyte valence, e is the elementary charge, n_0 is the concentration number of ions, and ω is the angular frequency.

Note that Eq. (A1) is general for a Newtonian fluid and can be applied to different cases: the real part is the response to a cosine time-varying applied electric field if $\omega \neq 0$, or to a DC electric field if $\omega = 0$, and the imaginary part is the response to a sinusoidal time-varying electric field ($\omega \neq 0$).

In the analysis considered in this work, we are interested in the velocity field response to a sine-wave input of the form $E(t) = E\sin(\omega t)$, thus at large times the imaginary part of Eq. (A1) gives the required velocity field:

$$\bar{u}(\bar{y},\bar{z},\bar{t}) = \frac{-64}{hw}\bar{G}\bar{E}\sum_{m=1}^{\infty}\sum_{n=1}^{\infty}C_{mn}\frac{R_{mn}\sin\left(\frac{\omega D_h^2}{\upsilon}\bar{t}\right)-\frac{4\omega}{\upsilon}\cos\left(\frac{\omega D_h^2}{\upsilon}\bar{t}\right)}{R_{mn}^2+\frac{16\omega^2}{\upsilon^2}} \times \cos\left[(2m-1)\frac{D_h}{w}\pi\bar{y}\right]\cos\left[(2n-1)\frac{D_h}{h}\pi\bar{z}\right] \tag{A.3}$$

where $R_{mn} = 4\pi^2\left(\frac{(2m-1)^2}{w^2}+\frac{(2n-1)^2}{h^2}\right)$

